RSC Advances




ROYAL SOCIETY OF CHEMISTRY

www.rsc.org/advances

RSC Advances

RSCPublishing

PAPER

# Performance enhancement of fullerene based solar cells upon NIR laser irradiation

Cite this: DOI: 10.1039/x0xx00000x

Hardeep Singh Gill,[a, b] Sammaiah Thota,[b] Lian Li,[c] Akshay Kokil, [b] Ravi Mosurkal,[c] and Jayant Kumar [a,b*]

Received 00th January 2015,
Accepted 00th January 2015

DOI: 10.1039/x0xx00000x

www.rsc.org/

Photovoltaic performance enhancement of fullerene based solar cells was achieved upon exposure to near-infrared (NIR) laser pulses. The solar cells were fabricated with poly(3-hexylthiophene) (P3HT) and [6,6]-phenyl $C_{61}$-butyric acid methyl ester (PCBM) under ambient condition. The cells were then post-treated with NIR femto-second laser pulses at 800 nm for different intervals of time. An enhancement of 50% in power conversion efficiency was achieved for the devices with 15 minutes of NIR laser irradiation compared to that of the control device. The enhancement in power conversion efficiency is attributed to the formation of covalent linkage between P3HT and PCBM as suggested by Matrix-assisted laser desorption/ionization time of flight mass spectroscopic analysis on a blend of a thiophene oligomer and PCBM before and after NIR laser exposure.

## 1. Introduction

Over the last two decades there has been worldwide initiative for the development of new renewable and sustainable energy sources using organic materials.[1-3] Organic materials based solar cells (OSCs) have been actively investigated as a possible alternative to inorganic solar cells. Bulk heterojunction (BHJ) structure, constitute of an interpenetrating network of a fullerene acceptor, such as [6,6]-phenyl-$C_{61}$ butyric acid methyl ester (PCBM) and a conjugated donor polymer, poly(3-hexylthiophene-2,5-diyl) (P3HT), as the photoactive layer, has been demonstrated to be the model OSC architecture.[3-6] Power conversion efficiency (PCE) up to 5% has been reported in solar cells fabricated from the blend of P3HT and PCBM.[7] The performance of the BHJ solar cell depends critically upon the morphology of the active layer. An optimized P3HT:PCBM OSC should consist of appropriate sized P3HT and PCBM phase-segregated nano-domains providing pathways for efficient charge carrier generation, transport and collection. However, the nanometer sized domains are metastable and degrade gradually under normal operating conditions, leading to severe degradation to the device performance.[8-11]

To address this problem, several PCBM-P3HT intramolecular hybrid polymers were designed and synthesized.[12-18]All those approaches have helped to optimize the morphology of the active layer and to reduce the PCBM aggregation, resulting in better stability of the OSCs.[14-17] It was previously reported that pristine fullerenes, such as $C_{60}$ and $C_{70}$, and their derivatives (PCBM and $PC_{70}BM$), can undergo photochemical transformation upon irradiation.[18-21] The fullerene monomers can be dimerized or oligomerized due to the formation of intermolecular C-C bonds between fullerenes via a '2+2' photochemical cycloaddition.[21] Recently, Li and co-workers reported the impact of photo-induced oligomerization of PCBM on the performance of the OSC.[22] Similar enhancement of the morphological stability following irradiation in the solar cells made with P3HT:PCBM and MDMO-PPV:PCBM, and PCDTBT:$PC_{70}BM$ has been reported.[23] The oligomerization of PCBM has been linked to the improved stability, but no explanation has been provided for the enhancement in efficiency. Moreover, due to strong visible light absorption of the polymers used, the low power visible radiation may not fully penetrate the active layer, thus the oligomerization of the fullerene monomers in the entire film would be difficult to achieve. Alternatively, high power laser pulses in the near-infrared (NIR) region could penetrate the entire active layer of the OSCs and would lead to better photochemical transformation of the fullerene molecules due to two-photon absorption,[24] resulting in enhanced stability.

In this work, we report on the PCE enhancement of the P3HT:PCBM solar cells and the possibility of the

covalent linkage between PCBM and P3HT upon the NIR laser irradiation. Raman analysis of the exposed samples revealed that the NIR laser irradiation was able to oligomerize the PCBM monomers. Exposure of the OSCs to the NIR laser pulses greatly stabilized the morphology in the active layer. An enhancement of 50% in PCE was achieved for the devices with 15 minutes of NIR laser irradiation compared to that of the control device. In addition, improvement in the photovoltaic stability was also observed. Matrix-assisted laser desorption/ionization time-of-flight mass spectroscopic (MALDI-TOF MS) analysis on a blend of a thiophene oligomer and PCBM before and after NIR laser exposure suggested the formation of '2+2' photochemical cycloaddition between thiophene oligomer and PCBM.

## 2. Experimental

### Materials and device fabrication

P3HT and PCBM were acquired from Sigma Aldrich and were first dissolved in 1,2-dichlorobenzene separately, and sonicated for 1 h. The two solutions were then mixed together. The concentration of mixed solution was about 20 mg/ml with a P3HT:PCBM weight ratio of 1:0.8. Indium-tin-oxide (ITO) coated glass substrates (10 Ω/□, purchased from Thin Film Devices) were patterned by chemical wet etching method using zinc dust and dilute HCl. The patterned substrates were cleaned in an ultrasonic bath with detergent, water, acetone and isopropanol, and dried in an oven. The substrates were further treated by oxygen plasma prior to casting the electron blocking PEDOT:PSS layer. The electron blocking layer about 40 nm thick was spin-coated at 2500 rpm from a heated (80 °C) and filtered (through a 0.45 µm membrane) PEDOT:PSS solution (Baytron P VP Al 4083) onto the cleaned ITO substrate. The PEDOT:PSS film was then dried at 120 ºC for 1 h. The mixed P3HT:PCBM solution was spin-coated at 800 rpm on the PEDOT:PSS covered ITO slides. The P3HT:PCBM films (~150 nm) were annealed at 120 ºC for 10 min under inert atmosphere immediately. An aluminium (Al) layer (120 nm) was thermally deposited onto the active layer through shadow mask in vacuum (about $10^{-6}$ mbar). The active area of the solar cells was 0.06 $cm^2$ defined by a shadow mask. Film thickness was determined with a Dektak profilometer.

### Spectroscopic and XRD Experiments

Raman measurements were carried out using a Bruker Senterra Raman microscope. The Raman spectra were measured using a green laser (532 nm, 2 mW). The laser beam diameter on the sample surface is about 1 µm. The spectral resolution of the spectrometer is about 3 $cm^{-1}$. All the Raman spectra were obtained with a data acquisition time of 5 s. The Raman spectra were background corrected using the Opus 6.5 software. Perkin-Elmer Lambda 9 spectrophotometer was used to measure the UV-Vis absorption spectra, and photoluminescence (PL) spectra were recorded using a Perkin-Elmer LS 55 luminescence spectrometer. For the PL experiment, the excitation wavelength was set at 530 nm. The spectral bandwidths for the excitation and emission were adjusted to 5 nm and 10 nm, respectively. Gated photomultiplier tube was used to collect the PL signal. Current-voltage (J-V) characteristics of the solar cells were measured under AM 1.5G solar illumination (100 $mW/cm^2$) with a Keithley 2400 source meter. Incident photon-to-current efficiency (IPCE) spectrum of the solar cells was measured using a CVI Digikrom 240 monochromator in conjunction with a water-cooled 150W Xe lamp (Model A-1010B, Photon Technology International, Inc.). Intensity of the incident illuminations was measured with a Newport 835 optical power meter. The photocurrent was collected by a Keithley 197 digital multimeter. X-ray diffraction (XRD) patterns were collected on a Scintag PAD X diffractometer in a Θ- 2Θ geometry with a water cooled Ge detector and a Cu Kα X-ray source (λ = 1.54 Å).

### Femtosecond laser Setup

A Quantronix mode-locked Ti:Sapphire laser operated at 800 nm with 100 femtosecond pulse width and 1 kHz repetition rate was used to irradiate the samples. The laser beam was expanded by a concave lens to completely illuminate the sample. The intensity of the laser beam was controlled to be about 15 $mW/cm^2$ using a neutral density filter.

### MALDI-TOF MS Measurements

MALDI-TOF MS data were acquired using a WATERS Micromass spectrometer. The instrument is equipped with a 337 nm pulsed nitrogen laser. TOF data from 20-50 individual laser pulses exposure were recorded and averaged on a transient digitizer, after which averaged spectra were automatically converted into mass by MassLynx data processing software. A thiophene oligomer, α-sexithiophene (molecular weight of 494.00 amu, purchased from Sigma-Aldrich), PCBM and a mixture of both materials were deposited on the MALDI target plates.

## 3. Results and discussion

The NIR laser exposed PCBM films in nitrogen environment along with unexposed films were characterized by Raman spectroscopy. For the pristine PCBM, the Raman peak of the Ag (2) "pentagonal pinch" mode at 1465 $cm^{-1}$ is very sensitive to the presence of the oligomerized phases. [25] Thus, the peak position of the Ag (2) mode can be used to distinguish the PCBM oligomers from the pristine monomeric PCBM. The PCBM oligomers exhibit a characteristic Raman peak at 1460 $cm^{-1}$. Fig. 1 shows the Raman spectra of the pristine and the irradiated PCBM films. Upon the NIR laser irradiation, the Raman peak at 1465 $cm^{-1}$ corresponding to the pristine PCBM monomer was down-shifted to 1460 $cm^{-1}$. This clearly indicated that the PCBM monomers were



 

oligomerized through covalent bonding with the neighbouring monomers. The PCBM oligomerization seems to have no significant impact on the photophysical properties of the PCBM and the P3HT:PCBM samples. No clear change of the absorption spectra of the laser exposed PCBM and P3HT:PCBM films in the nitrogen atmosphere was observed as compared to those of the non-irradiated samples (Fig. S1 and S2 in ESI†). XRD patterns of the thermally annealed (130 ºC, 1 h) laser exposed and the annealed control P3HT:PCBM samples were recorded and compared. As depicted in Fig. 2, both samples show very sharp and intense (100) reflection peak at 2 Θ = 5.4°, corresponding to the chain-chain interlayer distance.[26] Two weak (200) and (300) reflection peaks at 2 Θ = 10.7° and 15.9° were also detected, suggesting that the thiophene polymer in the blend film exhibit a well-organized intra-plane structure.[26] The (100) peak intensity of the laser exposed sample did not show any major change as compared to that of the control sample, indicating that laser irradiation does not disturb or change the crystallization of P3HT. These findings were also consistent with the results reported by Cheng et al.[27], where the authors have shown that the incorporation of polymerizable n-type materials does not appreciably affect the P3HT crystallinity of the blend.

The change in the PL characteristics of the sample is capable of probing the intermolecular electron transfer dynamics between donor and acceptor. The PL measurements of a P3HT film, the thermally annealed (130 ºC, 1 h) and un-annealed P3HT:PCBM samples, the NIR laser irradiated (5 and 15 minutes) and thermally treated P3HT:PCBM films were performed. Fig. 3 displays the PL spectra of the P3HT film, the annealed and un-annealed P3HT:PCBM films, and the irradiated and annealed P3HT:PCBM films. It is well-known that the PL from P3HT can be quenched by PCBM due to intermolecular electron transfer. The PL from P3HT in the un-annealed P3HT:PCBM film was significantly diminished due to quenching process. However, a strong PL signal for the annealed P3HT:PCBM film was measured. This is consistent with the observation of the formation of large PCBM aggregates (Fig. S3 and Fig. S4 in ESI†) in the film upon thermal treatment. The significant morphological changes result in less efficient charge transfer leading to weak quenching.[28,29] Weaker fluorescence was measured for the NIR laser and thermally treated P3HT:PCBM samples as compared to that from the annealed film. These results indicate that the NIR laser exposed films reduced the diffusion of PCBM molecules away from the polymer chains, resulting in lower PL intensities.

Enhancement in the photovoltaic performance of the BHJ-OSCs has been reported upon limited thermal annealing.[30] However; the thermal treatment can also reduce the interfacial surfaces between the polymer donor and the fullerene acceptor. This would also lead to inefficient charge separation and lower current output.[31] It is a great challenge to freeze the BHJ into optimized nano-phases architecture. To investigate the effect of NIR laser irradiation on the performance, solar cells were fabricated on ITO (as anode) coated glass substrates with P3HT:PCBM as active layer, poly (3,4-ethylenedioxythiophene):poly(styrenesulfonate)(PEDOT:PSS ) as the electron blocking layer and Al as the cathode. The cells were exposed to the NIR femtosecond laser beam with an intensity of 15 mW $cm^{-2}$ for different intervals of time in nitrogen atmosphere. The irradiated cells were then subject to thermal annealing at 120 ºC for 10 min along with the control cells. The J-V curves of all the devices were measured as shown in Fig. 4. The key photovoltaic characteristics are summarized in Table 1. The control cell yielded a PCE of 1.97% with a short-circuit current density ($J_{sc}$) of 6.97 $mA/cm^2$, an open-circuit voltage ($V_{oc}$) of 0.58 V, and a fill-factor (FF) of 0.48, respectively. As shown in Fig. 4, the NIR laser exposed solar cells exhibited significant improvement in the conversion efficiencies as compared to that of the control one. The device exposed to NIR-laser pulses for 15 min yielded a PCE of 2.90%. 50% enhancement in photovoltaic performance as compared to that of the control cell was achieved. The increase in PCE was mainly ascribed to the increase in $J_{sc}$ plus some improvement in FF. This drastic performance increase for the device with NIR light treatment is noteworthy, and has not been observed for the P3HT:PCBM solar cells. The IPCE spectra of the irradiated OSCs and the control device were measured. As shown in Fig. S5 (ESI†), the NIR laser treated OSCs exhibited enhanced external quantum efficiencies as compared to that of the control cell. This result suggested that the morphologies of the irradiated devices were better than that of the control cell and were able to offer favourable charge separation and transport. The NIR laser induced oligomerization of PCBM molecules prevented the monomers being diffused away from the P3HT matrix. It is noted that the sample temperature under the NIR laser exposure was measured to be about 35 ºC. This is significantly lower than the required annealing temperature, indicating that no thermal annealing occurred to the sample during irradiation.

The enhancement in the PCE for the NIR laser pulses treated devices was quite significant and the oligomerization of the PCBM molecules in the active layer could not be the only contributor. The NIR radiation could have induced a photochemical transformation causing a direct linkage between PCBM and P3HT and the molecular weight of P3HT would have increased. The direct linkage would offer more efficient way for charge separation. However, due to higher molecular weight of P3HT as compared to that of PCBM and the polydispersity of the polymer, it will be very difficult to notice any molecular weight change of the polymer by any mass spectrometer. The MALDI-TOF experiments were thus performed with a thiophene oligomer, α-sexithiophene, PCBM, and a mixture of α-sexithiophene and PCBM (1:1wt%) before and after exposure to the NIR laser pulses for 15 min in a nitrogen atmosphere to detect changes in molecular weights of the compounds. Formation of new chemical bonds between PCBM and α-sexithiophene after the laser exposure would lead to an increase of the molecular weight of the thiophene oligomer and should be reflected by

the emergence of new MALDI peaks corresponding to the molecular weights of the oligomer plus the weight(s) of PCBM monomer(s). The PCBM oligomer peak should be also be noticeable in the mass spectra.

Fig. S6 ((a) and (b)) in ESI† shows the MALDI-TOF mass spectra of the NIR laser exposed and pristine α-sexithiophene samples. The detection of molecular ion ($M^+$) peak at m/z 494.07 for both the pristine and NIR exposed α-sexithiophene samples revealed that the NIR laser irradiation did not cause any change to the thiophene oligomer. An $M^+$ peak at m/z 910 was observed for an unexposed PCBM sample as shown in the mass spectrum in Fig. S7(a) (ESI†). In addition, two fragmented mass ion peaks at m/z 720 (910-190) and 823 (910-87) were detected in the mass spectrum. The peak assignments of these fragments and parent structures are shown in Table S1 (ESI†). These peaks correspond to the mass of $C_{60}$, and the mass of PCBM with the loss of methyl ester group and two $CH_2$ groups from the side chain, respectively. The mass spectrum of the NIR laser irradiated PCBM sample (Fig. S7(b) in ESI†) showed an additional peak at m/z 1440 ($M^+$-380). This peak can be attributed to the major fragmentation peak of the dimerized PCBM occurred at the conjunction of the $C_{60}$ cage and phenyl-butyric acid methyl ester side chain. The mass spectrum of an unexposed blend α-sexithiophene:PCBM sample is depicted in Fig. 5 (a). The molecular ion ($M^+$) peaks of α-sexithiophene and PCBM were detected at m/z 494.07 and 910.1, 823, and 720, respectively. Fig. 5 (b) displays the mass spectrum of the NIR laser irradiated α-sexithiophene, PCBM mixed sample. Three additional peaks at m/z 1316.40, 1646.70 and 1805.73 were observed. The $M^+$ peak with maximum peak intensity at m/z 1316.40 (1404-88) as shown in Table 2 can be ascribed to the fragmentation of the two $-CH_2$ groups and methyl ester group ($-CO_2CH_3$) from the side chain of (2+2) cycloadduct between PCBM and α-sexithiophene ($M^+$-[$(CH_2)_2$ + ($-CO_2CH_3$)], 1404-88). The peaks at m/z 1646.70 and 1805.73 (Table 2) correspond to the fragmentation peaks of the dimerized PCBM resulting from the loss of two methyl ester groups and four $CH_2$ groups (1820-174), and a $CH_3$ group (1820-15), respectively.

The NIR laser irradiated photovoltaic devices also exhibited improved stability as compared to the control sample under ambient condition in the dark. It should be noted that no encapsulation was applied to all the solar cells. The key photovoltaic parameters for the 15 min NIR laser exposed cells and the control device were monitored with time up to 500 h. Fig. 6 displays their normalized $J_{sc}$, $V_{oc}$, FF and PCE as functions of time. After 500 h test, only 8% of the initial PCE value remained for the control cell. The observed decrease in the PCE mainly came from deterioration of both $J_{sc}$ and FF, while the $V_{oc}$ only dropped about 40%. However, dramatic improvement in stability for the NIR laser treated devices was measured and less than 30% of the original efficiency was lost. The stability evaluations for the fabricated cells with and without the NIR laser irradiation were also carried out to the fabricated organic solar cells at 80 ºC in dark. The key photovoltaic parameters of the fabricated devices as a function of time are shown in Fig. S8 (ESI†). Significant differences between the amount of performance degradation in the laser irradiated cells and the reference cells were observed. For the exposed samples, 88% of $J_{sc}$, 89% of FF and 95% of $V_{oc}$ were retained after heat treatment at 80 ºC for 200 h. The PCE of the exposed samples dropped to 1.15%, maintaining about 74% of its initial value. The control cells stopped working completely after 96 h heat treatment. These results clearly indicate that the NIR laser treatment can effectively improve the long term stability of the photovoltaic devices.

## 4. Conclusions

In summary, the P3HT:PCBM BHJ solar cells exhibited enhanced photovoltaic performance and stability when exposed to 100 femtosecond NIR laser irradiation. The improvement is attributed to the photochemical transformations in the active layer. The NIR light exposure leads to oligomerization of PCBM which then imparts better film morphological stability under thermal annealing. Covalent linkage between PCBM and thiophene polymer upon the laser irradiation could explain the enhancement of $J_{sc}$ and PCE due to improved charge separation.

## Acknowledgements

This work was supported as part of Polymer-Based Materials for Harvesting Solar Energy, an Energy Frontier Research Center funded by the U.S. Department of Energy, Office of Science, Basic Energy Sciences under Award #DE-SC0001087. This research was also supported by in part by an appointment to the Faculty Research Participation Program at the U.S. Army Natick Soldier Research, Development and Engineering Center (NSRDEC) administered by the Oak Ridge Institute for Science and Education through an interagency agreement between the U.S. Department of Energy and NSRDEC.

## Notes and references

[a]*Department of Physics, University of Massachusetts Lowell, Lowell, MA 01854.*
[b]*Center for Advanced Materials, University of Massachusetts Lowell, Lowell, Massachusetts 01854*
*Tel:9789343687; E-mail: Jayant_Kumar@uml.edu*

[c]*U.S. Army Natick Soldier Research, Development & Engineering Center, Natick, Massachusetts 01760, 9789343799, Lian_Li@uml.edu*

Electronic Supplementary Information (ESI) available: [details of any supplementary information available should be included here]. See DOI: 10.1039/b000000x/

## References

[1] S.B. Darling, F. You, *RSC Advances*, 2013, **3(39)**, 17633-17648.
[2] L.M. Peter, *Phys. Chem. Chem. Phys.*,2007, **9**, 2630-2642.



 

[3] G. Chamberlain, *Solar Cells*, 1983, **8**, 47-83.
[4] G. Dennler, M.C. Scharber, C.J. Brabec, *Adv. Mater.*, 2009, **21**, 1323-1338.
[5] S. Satapathi, H. S. Gill, L. Li, L. Samuelson, J. Kumar, R. Mosurkal, *Appl. Surf. Sci.*, 2014, **323**, 13-18.
[6] R. M. Osgood , K. M. Bullion , S. A. Giardini , J. B. Carlson , P. Stenhouse , R. Kingsborough, V. Liberman , L. Parameswaran , M. Rothschild , O. Miller , S. Kooi , J. Joannopoulos , F. Jeffrey , S. Braymen , H. Singh Gill , J. Kumar, *Proc. SPIE*, 2014, **9178**, 1-16.
[7] M.T. Dang, L. Hirsch, G. Wantz, P3HT: PCBM, *Adv. Mater.*, 2011, **23**, 3597-3602.
[8] K. Kawano, R. Pacios, D. Poplavskyy, J. Nelson, D.D. Bradley, J.R. Durrant, *Sol. Energ. Mat. Sol. Cells*, 2006, **90**, 3520-3530.
[9] M. Jørgensen, K. Norrman, F.C. Krebs, *Sol. Energ. Mat. Sol. Cells*, 2008, **92**, 686-714.
[10] E. Klimov, W. Li, X. Yang, G. Hoffmann, J. Loos, *Macromolecules*, 2006, **39**, 4493-4496.
[11] M. Bag, T.S. Gehan, L.A. Renna, D.D. Algaier, P. M. Lahti, D. Venkataraman, *RSC Advances*, 2014, **4(85)**, 45325-45331.
[12] J.U. Lee, J.W. Jung, T. Emrick, T.P. Russell, W.H. Jo, *Nanotechnology*, 2010, **21**,105201.
[13] C. Yang, J.K. Lee, A.J. Heeger, F. Wudl, *J. Mater. Chem.*, 2009, **19**, 5416-5423.
[14] B. Gholamkhass, T.J. Peckham, S. Holdcroft, *Polym. Chem.*, 2010, **1**, 708-719.
[15] J. U. Lee, A. Cirpan, T. Emrick, T. P. Russell, W. H. Jo, *J. Mater. Chem.*, 2009, **19(10)**, 1483-1489.
[16] C. Li, H. Yip, A.K. Jen, *J. Mater. Chem.*, 2012, **22**, 4161-4177.
[17] M. Chen, M. Li, H. Wang, S. Qu, X. Zhao, L. Xie, S. Yang, *Polym. Chem.*, 2013, **4**, 550-557.
[18] P. Eklund, A. Rao, P. Zhou, Y. Wang, J. Holden, *Thin Solid Films*, 1995, **257**, 185-203.
[19] A. Rao, P. Zhou, K. Wang, G. Hager, J. Holden, Y. Wang, W. Lee, X. Bi, P. Ecklund, D. Cornett, *Science*, 1993, **259**, 955-957.
[20] J. Wang, C. Larsen, T. Wågberg, L. Edman, Direct UV patterning of electronically active fullerene films, *Adv. Funct. Mater.*, 2011, **21**, 3723-3728.
[21] A. Dzwilewski, T. Wågberg, L. Edman, *J. Am. Chem. Soc.*, 2009, 131, 4006-4011.
[22] Z. Li, H.C. Wong, Z. Huang, H. Zhong, C.H. Tan, W.C. Tsoi, *Nat. Commun.*, 2013, **4**.
[23] F. Piersimoni, G. Degutis, S. Bertho, K. Vandewal, D. Spoltore, T. Vangerven, J. Drijkoningen, M.K. Van Bael, A. Hardy, J. D'Haen, *J. Polym. Sci. Part B: Polym. Phys.*, 2013, **51**, 1209-1214.
[24] B. Taheri, H. Liu, B. Jassemnejad, D. Appling, R. C. Powell, J. Song, *Appl. Phys. Lett.*, 1996, **68(10)**,1317-1319.
[25] A. Dzwilewski, T. Wågberg, L. Edman, *J. Am. Chem. Soc.*, 2009, **131**, 4006-4011.
26 J. Uk. Lee, J. W. Jung, T. Emrich, T. P. Russell, W. H. Jo, *Nanotechnology*, 2010, **21(10),** 105201.
[27] Y. J. Cheng, C.H. Hsieh, P. J. Li, C. S. Hsu, *Adv. Funct. Mater.*, 2011, **21(9)**, 1723-1732.
[28] S. S. Van Bavel, M. Bärenklau, G. de With, H. Hoppe, J. Loos, *Adv. Funct. Mater.*, 2010, **20(9)**, 1458-1463.
[29] Y. Xie, Y. Li, L. Xiao, Q. Qiao, R. Dhakal, Z. Zhang, Q. Gong, D. Galipeau, X. Yan, *J. Phys. Chem. C.*, 2010, **114**,14590-14600.
[30] G. Sharma, P. Suresh, S. Sharma, Y. Vijay, J.A. Mikroyannidis, *ACS Appl. Mater. Interfaces*, 2010, **2**, 504-510.
[31] G. Li, V. Shrotriya, Y. Yao, Y. Yang, *J. Appl. Phys.*, 2005, **98**, 043704.

## Figures and Tables

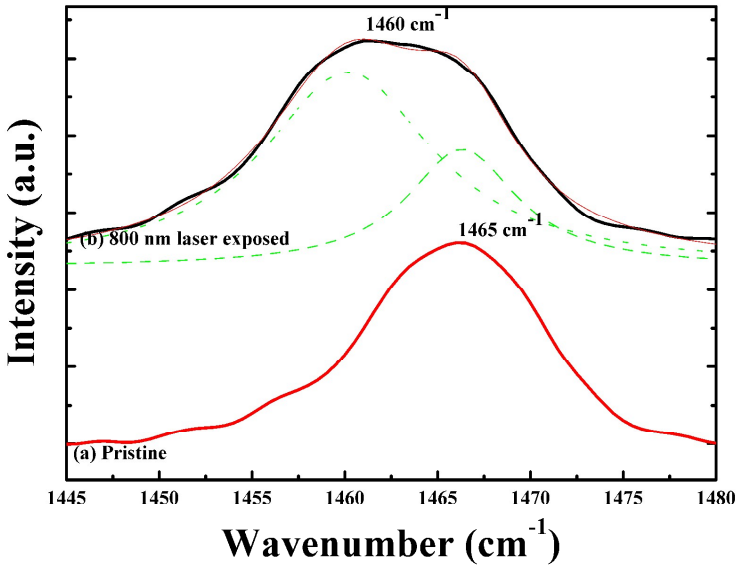


**Fig. 1** Raman spectra of (a) a pristine PCBM film and (b) a PCBM film after NIR laser irradiation for 15 minutes. The dash lines were fitted with two Lorentzian functions with peak positions at 1460 $cm^{-1}$ for oligomerized PCBM and at 1465 $cm^{-1}$ for pristine PCBM, respectively.

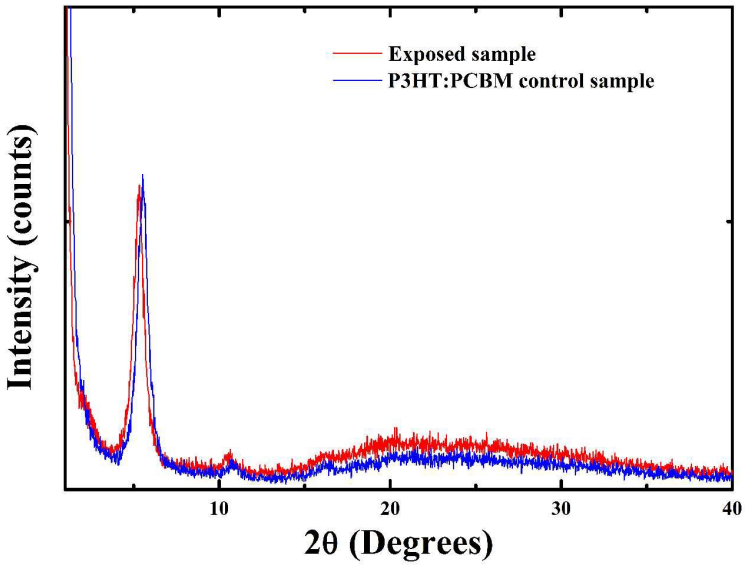


**Fig. 2** XRD patterns of a P3HT:PCBM film annealed at 130 ºC for 1 h and a P3HT:PCBM film after 15 min exposure to NIR laser and annealed at 130 ºC for 1 h.

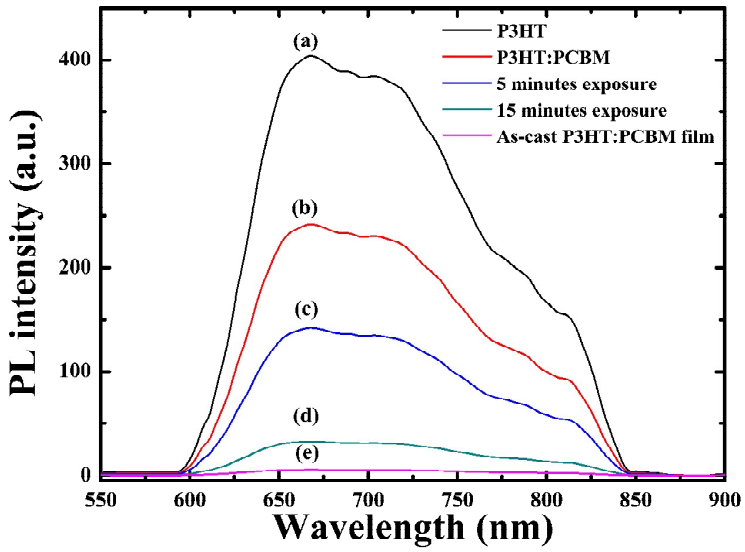


**Fig. 3** PL spectra of (a) a P3HT film, (b) a P3HT:PCBM film annealed at 130 ºC for 1 h, (c) a P3HT:PCBM film after 5 min exposure to NIR laser and annealed at 130 ºC for 1 h, (d) a P3HT:PCBM film after 15 min exposure to NIR laser and annealed at 130 ºC for 1 h, and (e) a non-exposed and un-annealed P3HT:PCBM film.

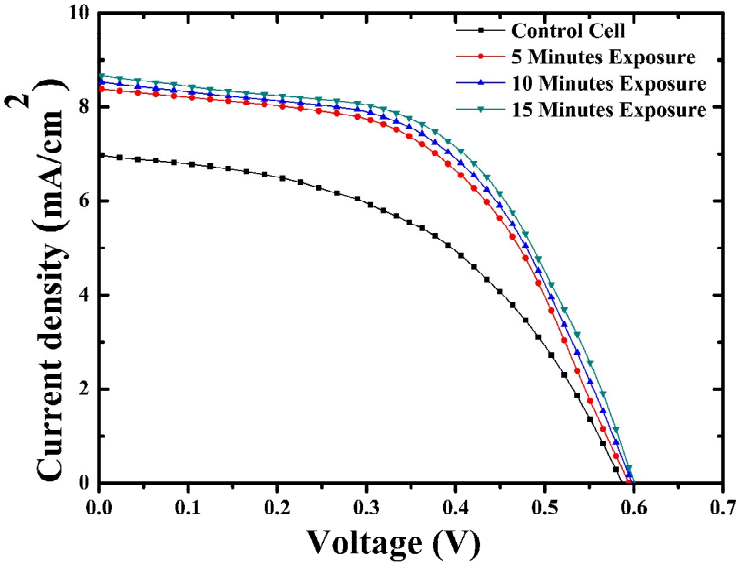


**Fig. 4** J-V characteristics of the BHJ-OSCs without (filled squares) and with 5 min (filled circles), 10 min (filled triangles), and 15 min (filled inverted triangles) exposure to NIR laser pulses.

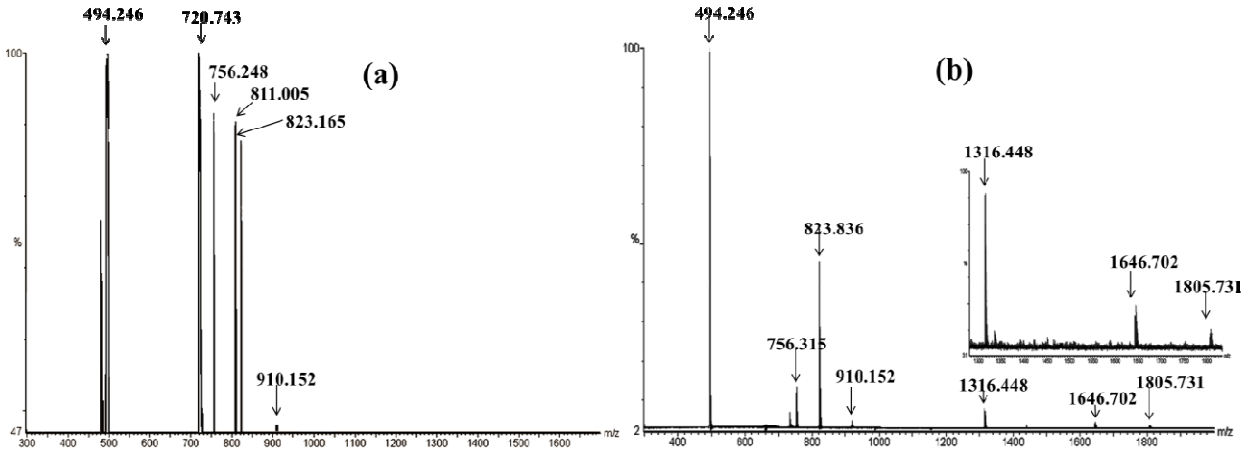


**Fig. 5** MALDI-TOF spectra of the (a) α-sexithiophene:PCBM blend sample and(b) α-sexithiophene:PCBM blend sample after exposure to NIR laser irradiation.

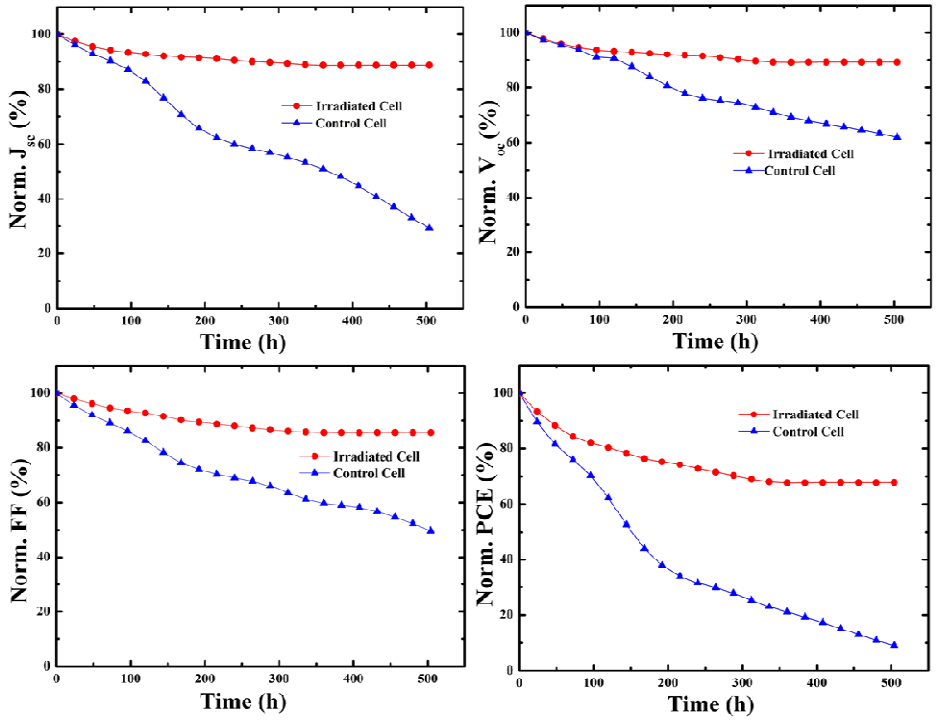


**Fig. 6.** Stability evaluation of the 15 min NIR laser exposed solar cell as compared to the control cell under ambient condition.

## Tables

**Table 1.** OSC performance characteristics.

| Sample | Jsc ($mA/cm^2$) | Voc (V) | FF (%) | Eff. (%) | $R_{series}$ ($ohm/cm^2$) | $R_{shunt}$ ($ohm/cm^2$) |
|---|---|---|---|---|---|---|
| Control | 6.9±0.07 | 0.586±0.03 | 48.3±0.03 | 1.97±.01 | 25.3±0.8 | 382±8 |
| 5 minutes | 8.37±0.04 | 0.596±0.02 | 53.4±0.02 | 2.68±.01 | 25.2±0.8 | 532±9 |
| 10 minutes | 8.49±0.04 | 0.601±0.02 | 54.1±0.02 | 2.79±0.2 | 21.9±0.9 | 510±9 |
| 15 minutes | 8.68±0.05 | 0.606±0.02 | 54.8±0.02 | 2.90±0.1 | 19.3±0.8 | 490±9 |

The photovoltaic parameters were the average of four devices in the same batch. Short-circuit current density, open-circuit voltage, fill factor, power conversion efficiency, series and shunt resistance were derived from the J-V curves in Fig. 4.

**Table 2.** Structural assignment of peaks observed in MALDI-TOF mass spectra.

| | | | | |
|---|---|---|---|---|
| Chemical structures of Possible Chemical fragments | 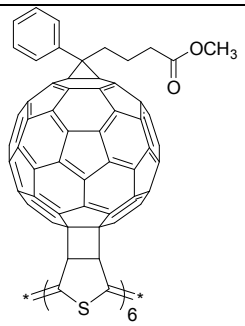 | 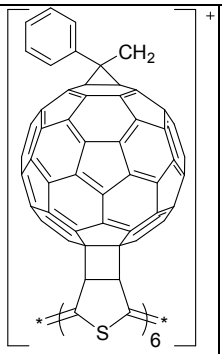 | 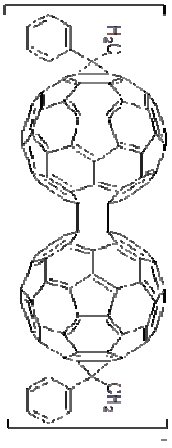 | 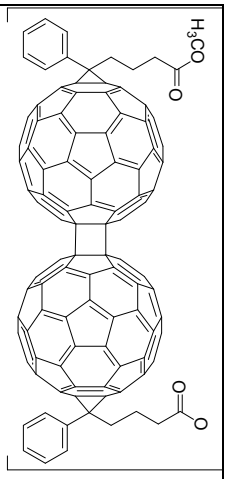 |
| Theoretical (m/z) | 1404 | 1316 | 1646 | 1805 |
| Observed MALDI-TOF (m/z) | 1404 | 1316.448 | 1646.702 | 1805.731 |